Model order reduction techniques applied to magnetodynamic scalar potential formulation

Fabian Müller
Institute of Electrical Machines (IEM)
RWTH Aachen University
Aachen, Germany
fabian.mueller@iem.rwth-aachen.de

Lucas Crampen
Institute of Electrical Machines (IEM)
RWTH Aachen University
Aachen, Germany

Thomas Henneron
L2EP
Université de Lille
Lille, France

Stéphane Clénet
L2EP
Ecole Nationale Supérieure d'Arts et Métiers
Lille, France

Kay Hameyer
Institute of Electrical Machines (IEM)
RWTH Aachen University
Aachen, Germany

***Abstract*—Numerical techniques to extract important information from large systems of equations are in focus of research to cope with the computational effort. This paper discusses the feasibility of model order reduction techniques applied to magnetic scalar potential formulation coupled to the electric vector potential, known as $\boldsymbol{T}-\boldsymbol{\Omega}$ formulation. This formulation, compared to the magnetic vector potential formulation, uses a decomposition of the magnetic field into a scalar potential and loop fields to avoid explicit cuts, necessary to not violate Ampère's law. The analysis of different techniques, namely the Proper Orthogonal Decomposition and Proper General Decomposition, applied to a three dimensional eddy current problem are performed. The presented approach is finally evaluated in terms of convergence and computational efforts.**

***Index Terms*—Proper general decomposition (PGD), proper orthogonal decomposition (POD), reduced order systems, $\boldsymbol{T}-\boldsymbol{\Omega}$ formulation, model order reduction, MOR**

I. Introduction

Transient electromagnetic field phenomena are commonly solved by the Finite Element Method (**FEM**) employing the magnetic vector potential formulation, due to its good numerical representation of field quantities. Nevertheless another approach can be performed by introducing the magnetic scalar potential Ω and the electric vector potential $\boldsymbol{T}$, resulting in a smaller system while maintaining the accuracy. Particularly for linear eddy current problems the $\boldsymbol{T}-\Omega$ is well suited. To cope with the resulting computational effort of solving many linear equation systems, model order reduction (**MOR**) can be employed. Even though the Proper Orthogonal Decomposition (**POD**) is widely applied [1], [2] and the Proper Generalized Decomposition (**PGD**) has also shown its capability to solve many numerical problems [1], [3], [4], a scientific analysis of POD and PGD in combination with the $\boldsymbol{T}-\Omega$ method is pending. For this purpose the necessary fundamentals of the two methods are explained in detail with a focus from an implementational point of view. Consecutively the convergence as well as the computational effort of the methods are illustrated.

This work was supported by the German Research Foundation (DFG) within the research project number 347941356 "Numerical Analysis of Electromagnetic Fields by Proper Generalized Decomposition in Electrical Machines".

II. Magnetodynamic Finite Element Formulation

For the utilization of the magnetic scalar potential formulation the magnetic field strength has to be represented by the electric vector potential $\boldsymbol{T}$ and the magnetic scalar potential Ω (1).

$$\boldsymbol{H} = \boldsymbol{T} - \nabla\Omega \tag{1}$$

The electric vector potential $\boldsymbol{T}$ is defined by the sum of the exciting vector potential $\boldsymbol{T}_0$ and the eddy current component $\boldsymbol{T}_\mathrm{e}$ (2).

$$\boldsymbol{T} = \boldsymbol{T}_0 + \boldsymbol{T}_\mathrm{e} \tag{2}$$

Considering Faraday's law leads to (3) containing the unknowns $\boldsymbol{T}_e$ and Ω.

$$\nabla \times (\frac{1}{\sigma}\nabla \times \boldsymbol{T}_\mathrm{e}) + \frac{\partial \mu \boldsymbol{T}_\mathrm{e} - \partial \mu \nabla\Omega}{\partial t} = -\frac{\mu \partial \boldsymbol{T}_0}{\partial t} \tag{3}$$

The second equation to be considered originates from the conservation of the magnetic fluxdensity in combination with the material equation for the magnetic field strength and is stated in (4).

$$\nabla \cdot (\mu \boldsymbol{T}_\mathrm{e}) - \nabla \cdot (\mu \nabla\Omega) = -\nabla \cdot (\mu \boldsymbol{T}_0) \tag{4}$$

In this context the exciting current vector potential is defined by the application of a spanning tree technique [5]. Considering a domain G, containing a simply connected conductive region G_c the formulation above can be applied. The introduced magnetic scalar potential is expressed by nodal elements, while the electric vector potential is expressed in the edge element space. To obtain the weak formulation, the Galerkin method is applied. Further a tree-cotree gauge in the sample is employed [6].

III. Model Order Reduction

The POD as well as the PGD are based on the approach that the unknown potentials can be decomposed into products of functions, that depend on one variable such as space or time (5) [1], [4]. In equation (5) the vector $\boldsymbol{U}$ represents $\boldsymbol{T}_e$, respectively $\boldsymbol{\Omega}$, with a finite number m of terms. These terms are also commonly called modes.

$$\boldsymbol{U} \approx \sum_{i=1}^{m} \boldsymbol{R}_{\mathrm{i}}(\boldsymbol{x}) S_{\mathrm{i}}(t) \tag{5}$$

$\boldsymbol{R}(\boldsymbol{x})$ is defined in the edge, respectively nodal element space, while $S(t)$ is defined on the studied time interval.

A. Proper Orthogonal Decomposition

The POD is an a-posteriori approach, meaning that it builds its reduction by taking information from previously generated solutions in the reference system and creation of a projection operator. This projection is applied onto the reference system to receive a reduced representation [1], [2], [7].

1) Building the projection: To achieve a reduction in terms of degrees of freedom (**DOF**), the solution vector $\boldsymbol{X}$, which contains $\boldsymbol{T}$ and Ω, is estimated with a new solution vector $\boldsymbol{X}_{\mathrm{r}}$ of smaller size [12].

$$\boldsymbol{X} \approx \mathbf{P}\boldsymbol{X}_{\mathrm{r}} \tag{6}$$

In equation (6), P denotes a projection operator which projects the system of size number of unknowns n into a reduced system with the size m ($m << n$). The projection P is constructed by employing the method of snapshots. The reference system is solved for k time steps and the solutions are stored in the snapshot matrix $\mathbf{A}_{\mathrm{S}} = [\boldsymbol{X}_1, \boldsymbol{X}_2, ..., \boldsymbol{X}_{\mathrm{k}}]$ of size $n \times k$, where k is equal to the number of snapshots (**NoS**). Furthermore, there are different strategies which m of those k calculated solutions should be taken to create the projection, shown in the following section. Consecutively the resulting snapshot matrix $\mathbf{A}_{\mathrm{S}}$ of size m has to be evaluated in terms of a Singular Value Decomposition (**SVD**). For systems with many DOF, this leads to an ambitious computational effort. Using the relation between SVD of a given matrix $\mathbf{A}_{\mathrm{S}}$ (7) and the eigenvalue decomposition of the correlated quadratic matrix $\mathbf{C}_{\mathrm{S}}$ (8) [8], significantly reduces the computational effort. Finally the Projection operator can be achieved by (9).

$$\mathbf{A}_{\mathrm{S}} = \mathbf{V}\boldsymbol{\Sigma}\mathbf{W}^{\mathrm{t}} \tag{7}$$

$$\mathbf{C}_{\mathrm{S}} = \frac{1}{m}\mathbf{A}_{\mathrm{S}}^{\mathrm{t}}\mathbf{A}_{\mathrm{S}} = \mathbf{W}\boldsymbol{\Delta}\mathbf{W}^{\mathrm{t}} \tag{8}$$

$$\boldsymbol{P} = \mathbf{V}\boldsymbol{\Sigma} = \mathbf{A}_{\mathrm{S}}\mathbf{W} \tag{9}$$

Subsequently achieve the reduced system the projection has to be applied to the reference equation

$$\mathbf{P}^{\mathrm{t}}\mathbf{M}\mathbf{P}\boldsymbol{X}_{\mathrm{r}} = \mathbf{P}^{\mathrm{t}}\boldsymbol{F}(t)\ . \tag{10}$$

In Equation (10) $\mathbf{M}$ is the system matrix and $\boldsymbol{F}(t)$ is the right hand side, given by the weak form of (3) and (4).

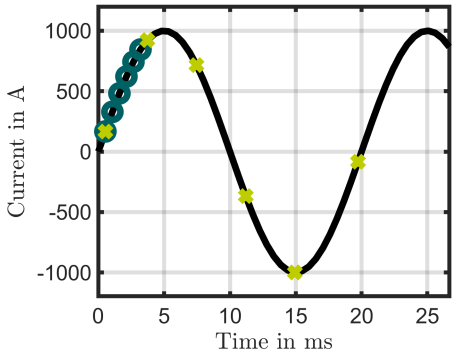

Fig. 1: Snapshots taken for the two presented methods; circle = sequential, cross = system based.

2) Snapshot Method: A direct consequence of the projection creation (9) is the influence of the snapshots on the accuracy of the reduced system. By applying the SVD on the snapshot matrix, the solution space is explored. If the computed solutions, for example, contain the same vector twice or just a few very similar ones, the decomposition will not produce accurate results. The SVD extracts rotating and scaling given in the matrix $\mathbf{A}_{\mathrm{S}}$ and for this reason mutually different snapshots are preferable. Two common routines for taking snapshots are illustrated in the following. Obviously the method with less computational effort is given by subsequently taking snapshots for a certain amount of time steps. As previously delineated, this method can lead to inaccuracies, if the snapshots are very similar. The method is depicted in Fig. 1.

The second method is the system based approach. Due to the transient behaviour, the first m time steps will probably not sought all relevant information into the reduced model, therefore, taking evenly distributed snapshots will produce more accurate results. A trade of between computational effort and accuracy is achieved by distributing the snapshots only in the first current period. For static problems greedy algorithm based snapshot method can be used to further improve the decomposition but are unfeasible in terms of computational effort in context of eddy current problems [9].

B. Proper Generalized Decomposition

The PGD is an a-priori approach and it is characterized by a substitution of $\boldsymbol{T}$ and Ω with the approach stated in (5) [1]-[4]. Consecutively the basis functions of the weak formulation are substituted as well by (11), (12). Hereby $\boldsymbol{\alpha}$ represents the nodal test functions, while $\boldsymbol{\beta}$ represents the edge element test functions.

$$\boldsymbol{\alpha} = \boldsymbol{R}_{\Omega}(\boldsymbol{x})^{'} S_{\Omega}(t) + \boldsymbol{R}_{\Omega}(\boldsymbol{x}) S_{\Omega}(t)^{'} \tag{11}$$

$$\boldsymbol{\beta} = \boldsymbol{R}_{\mathrm{T}}(\boldsymbol{x})^{'} S_{T}(t) + \boldsymbol{R}_{\mathrm{T}}(\boldsymbol{x}) S_{T}(t)^{'} \tag{12}$$

The computation of the single modes is done in an alternating way by assuming that the space or time function is known. The whole iteration process is illustrated in Fig. 2, which is

repeated until a relative convergence is met or a maximum number of nonlinear iterations (**maxNL**) is hit. By knowing one of those, the test function belonging to the known component vanishes in (11), (12). Assuming that the modes up to m-1 are known, the evaluation of the space functions can be achieved by solving the differential algebraic equations (13), (14) with the FEM. $\boldsymbol{T}_{0,\boldsymbol{x}}$ / $\boldsymbol{T}_{0,t}$ denotes the space and time part of the excitation respectively.

$$\begin{aligned}
&\sum_{i=1}^{m}\int_{G_\mathrm{c}}\frac{1}{\sigma}\nabla\times\boldsymbol{R}_{\mathrm{T,i}}\nabla\times\boldsymbol{R}_{\mathrm{T}}^{'}\,\mathrm{d}G_c\int_t S_{\mathrm{T,i}}S_{\mathrm{T,m}}\mathrm{d}t\\
&+\sum_{i=1}^{m}\int_{G_\mathrm{c}}\mu\boldsymbol{R}_{\mathrm{T,i}}\boldsymbol{R}^{'}{}_{\mathrm{T}}\,\mathrm{d}G_c\int_t\frac{\partial S_{\mathrm{T,i}}}{\partial t}S_{\mathrm{T,m}}\mathrm{d}t\\
&-\sum_{i=1}^{m}\int_{G}\mu\nabla\boldsymbol{R}_{\Omega,\mathrm{i}}\boldsymbol{R}_{\mathrm{T}}^{'}\,\mathrm{d}G\int_t\frac{\partial S_{\Omega,\mathrm{i}}}{\partial t}S_{\mathrm{T,m}}\mathrm{d}t\\
&=-\int_{G}\mu\boldsymbol{T}_{0,\boldsymbol{x}}\boldsymbol{R}_{\mathrm{T}}^{'}\mathrm{d}G\int_t\frac{\partial T_{0,\mathrm{t}}}{\partial t}S_{\mathrm{T}}\mathrm{d}t \qquad (13)\\
&\sum_{i=1}^{m}\int_{G_\mathrm{c}}-\mu\nabla\boldsymbol{R}_{\Omega}^{\prime}\boldsymbol{R}_{\mathrm{T,i}}\,dG_c\int_t S_{\Omega,m}S_{\mathrm{T,i}}\mathrm{d}t\\
&+\sum_{i=1}^{m}\int_{G}\mu\nabla\boldsymbol{R}_{\Omega,\mathrm{i}}\nabla\boldsymbol{R}_{\Omega}^{\prime}\mathrm{d}G\int_t S_{\Omega,\mathrm{i}}S_{\Omega,\mathrm{m}}\mathrm{d}t\\
&=-\int_{G}\mu\nabla\boldsymbol{R}_{\Omega}^{\prime}\boldsymbol{T}_{0,\boldsymbol{x}}\mathrm{d}G\int_t S_{\Omega,\mathrm{m}}T_{0,\mathrm{t}}\mathrm{d}t \qquad (14)
\end{aligned}$$

To determine the time functions the previously calculated space functions are fixed and the time functions are taken as unknowns, resulting in a system of ordinary differential equations (ODE). The space test functions vanish and insertion of (11), (12) into the $\mathbf{T}-\Omega$ formulation results in (15), (16).

$$\begin{aligned}
&\sum_{i=1}^{m}\int_{G_\mathrm{c}}\frac{1}{\sigma}\nabla\times\boldsymbol{R}_{T,i}\nabla\times\boldsymbol{R}_{T,m}\,dG_c\,S_{T,i}\\
&+\sum_{i=1}^{m}\int_{G_\mathrm{c}}\mu\boldsymbol{R}_{T,i}\boldsymbol{R}_{T,m}\,dG_c\,\frac{\partial S_{T,i}}{\partial t}\\
&-\sum_{i=1}^{m}\int_{G}\mu\nabla\boldsymbol{R}_{\Omega,i}\boldsymbol{R}_{T,m}dG\,\frac{\partial S_{\Omega,i}}{\partial t}\\
&=-\int_{G}\mu\boldsymbol{T}_{0,\boldsymbol{x}}dG\frac{\partial T_{0,t}}{\partial t} \qquad (15)\\
&-\sum_{i=1}^{m}\int_{G_\mathrm{c}}\nabla R_{\Omega,m}R_{T,i}\,dG_c\,S_{T,i}\\
&+\sum_{i=1}^{m}\int_{G}\mu\nabla R_{\Omega,i}\nabla R_{\Omega,m}\mathrm{d}G\,S_{\Omega,i}\\
&=\int_{G}\mu\nabla R_{\Omega,m}\boldsymbol{T}_{0,\boldsymbol{x}}\mathrm{d}G\,T_{0,t} \qquad (16)
\end{aligned}$$

The ODE can be solved in its strong form by using suitable solvers for e.g. an implicit Euler method. To improve the relative convergence of the enrichment process the time functions are normalized to prevent cases in which one part of the decomposition tends to become infinitely small while the other one diverges towards infinity.

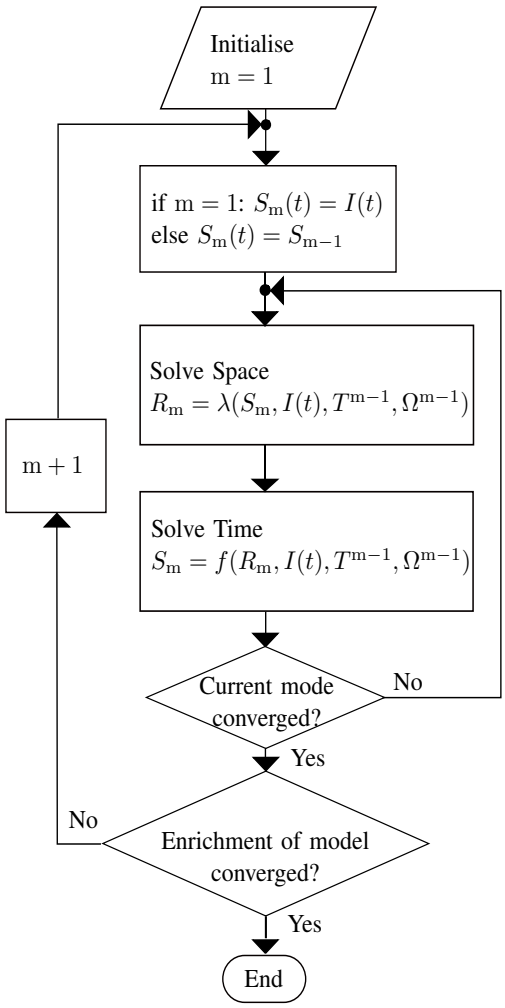

Fig. 2: Alternating scheme to determine linear PGD representation.

C. Convergence and Error Evaluation

After the reduced representations have been achieved the convergence and the error needs to be evaluated. Therefore an physical error criteria, based on the Joule losses in the sample (17), is applied. Due to the necessity of reference values this is an a-posteriori criteria.

$$\epsilon_j = \frac{||P_{j,ref} - P_{\mathrm{j,MOR}}||_2}{||P_{\mathrm{j,ref}}||_2} \qquad (17)$$

IV. Application

The $\boldsymbol{T}-\Omega$ formulation is in this context applied to solve an academic example of a conducting sample located inside a short coil (Fig. 3). The model is computed with two different conductivities of $4\,\mathrm{MS/m}$ and $40\,\mathrm{MS/m}$. Therefore, this example is similar to an induction furnace, in which the eddy currents can be used for heating a probe. The occuring eddy currents are proportional to the frequency and conductivity and will diffuse from the outside into the probe. To properly model the eddy currents the skin depth has to be accurately

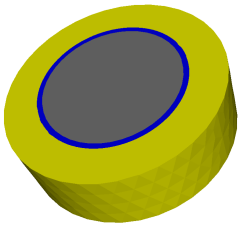

Fig. 3: Academic example of an eddy current problem (Coil = yellow, sample = grey, airgap = blue).

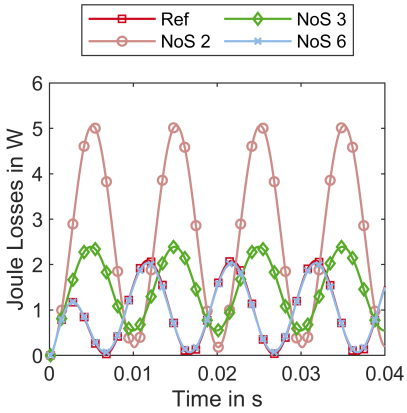

Fig. 4: Joule losses over time for POD taking sequential snapshots.

discretized. The simulation frequency is set to 50 Hz and the sinussoidal current has a magnitude of 100 A. The magnetic permeability is set to μ_0 and the reference solutions are obtained by a classic time stepping simulation. There number of time steps (**NoT**) for the investigated intervall is set to 300.

A. Results - POD

In Fig. 4 the evolution of the Joule losses over time is shown. For the sequential snapshot method, six snapshots are sufficient to receive an error smaller than 2% for a given conductivity of $40\,\mathrm{MS/m}$. It is obvious that the Joule Losses are not accurate for lower numbers of snapshot. The Joule error (17) for the sequential snapshots is shown in Fig. 5. Due to the transient eddy currents, which are proportional to the conductivity less snapshots are necessary for an accurate representation of the losses for $4\,\mathrm{MS/m}$ compared to $40\,\mathrm{MS/m}$. The convergence is given for both conductivity and is linear. The system based approach produce a decomposition, which shows higher accuracy with less modes. The evolution of the system based POD Joule losses behaves differently compared to the sequential approach. In Fig. 6 the losses are illustrated over the time of two current periods. The convergence rate of the POD with system based snapshots is much faster compared to the sequential snapshots. It can be depicted from Fig. 7 that three snapshots are enough to reproduce the eddy current losses for a conductivity of $4\,\mathrm{MS/m}$ with an error smaller

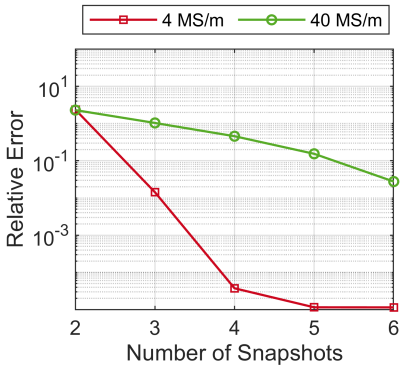

Fig. 5: Error of Joule losses for sequential POD.

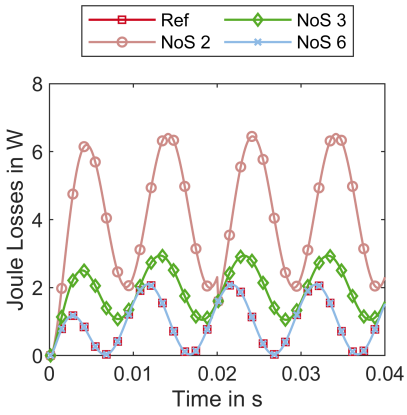

Fig. 6: Joule losses over time for POD taking system based snapshots.

than 2e-5 and for four snapshots the error drops below 1e-5. Also the losses for the higher conductivity of $40\,\mathrm{MS/m}$ are more accurate than those of the sequential snapshots approach. While the error of the sequential approach with four modes is higher than 20%, the error of the system based approach is smaller than 1e-4. Comparing the Joule losses of the two different snapshot methods, it is noticeable that the system

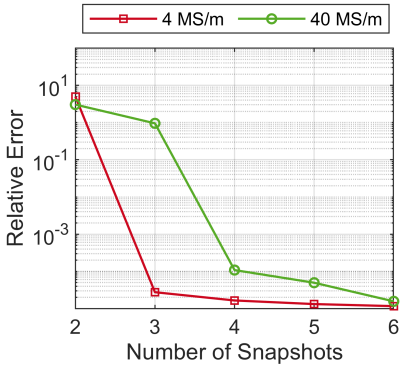

Fig. 7: Error of Joule losses for system based POD.

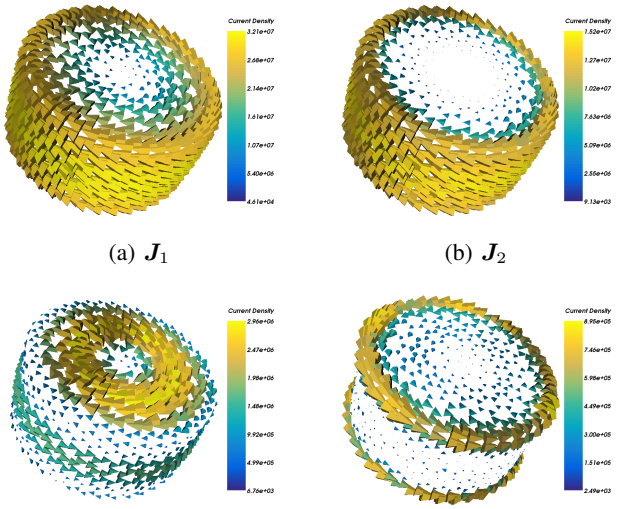

(a) $\boldsymbol{J}_1$ (b) $\boldsymbol{J}_2$

(c) $\boldsymbol{J}_3$ (d) $\boldsymbol{J}_4$

Fig. 8: Eddy current modes of the PGD.

based approach captures more relevant information of the transient effect with less number of snapshots, see Fig. 1. This improvement in terms of accuracy comes with the price of more computations in the reference system. For the sequential approach only **NoS** computations in the reference system has to be done, while the system based approach needs the full first current period simulated in the reference system.

B. Results - PGD

Due to the direct decomposition of the PGD, the space and time modes can be analysed directly. The first four computed space modes for a conductivicty of $40\,\mathrm{MS/m}$ are shown in Fig. 8. It can be depicted that the first mode is a uniformly rotating eddy current, while the second mode only has an eddy current on the side, which is decreasing towards the center of the sample. The third mode shows an interesting phenomenon: The eddy currents at the top and bottom of the sample are rotating clockwise with a maximum at half of the sample radius. Moreover at the side of the sample, a counterclockwise rotating eddy current is visible. This can be interpreted as follows: The first mode acts like an eddy current in low conductive samples, while the second mode increases the eddy current in the edge region. The third mode decreases the field in the middle of the sample. In combination with the enriched time functions, shown in Fig. 11, the diffusion of the eddy current into the sample can be modelled by the linear combination given by (5). All functions show a transient behaviour. In combination with the decreasing amplitude of the space modes, it can be assumed that the first two modes have a large impact on the overall behaviour of the eddy currents, while the third and later are more or less diminishing errors smaller errors of the transient simulation. The Joule losses of the PGD, depending on the number of modes (**NoM**), are shown in Fig. 9. In contrast to the Joule losses computed

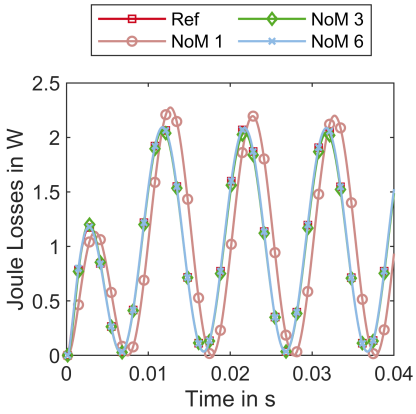

Fig. 9: Joule losses over time for PGD taking system based snapshots.

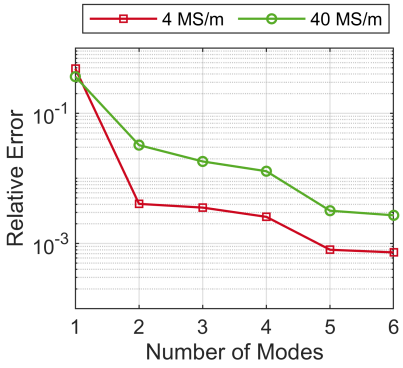

Fig. 10: Error of Joule losses for PGD.

with the POD, the first mode of the PGD contains the most dominant information of the electric vector potential $\boldsymbol{T}$. The latter modes correct the amplitude and phase. The convergence of the error between the PGD and the reference losses is not as smooth as the convergence of the POD, but still a quasi linear convergence rate can be depicted. For a conductivity of $4\,\mathrm{MS/m}$ the first mode produces an error of approximately 20% while the error of both POD methods with two snapshots is bigger than 100%. Similar to the POD methods, it can be seen that the error for the lower conductivities decreases faster than for the higher one.

Consecutively to the Joule loss evaluation, a direct comparison of the three MOR methods for a conductivity of $40\,\mathrm{MS/m}$ shall be done here. In Fig. 12 the error (17) for all methods is illustrated and two fundamental aspects can be recognized;

TABLE I: Computations of MOR for a transient Problem

Operation	**Ref**	**PGD**	**POD**
Build Ref. O(n^2)	NoT	NoM·maxNL	NoT
Solve Ref. O(n^2)	NoT	NoM·maxNL	NoS
Solve Red. O(NoS^2)	0	0	(NoT-NoS)
Multi. O(n)	0	NoT·NoM	4·(NoT-NoS)

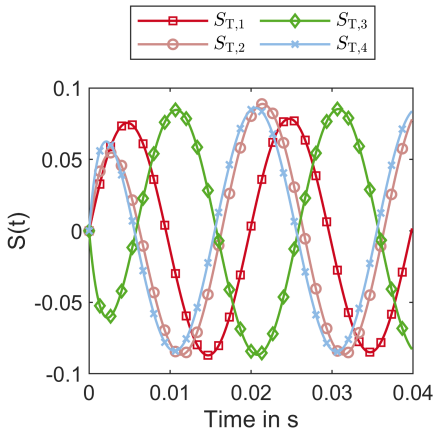

Fig. 11: Time functions of the PGD.

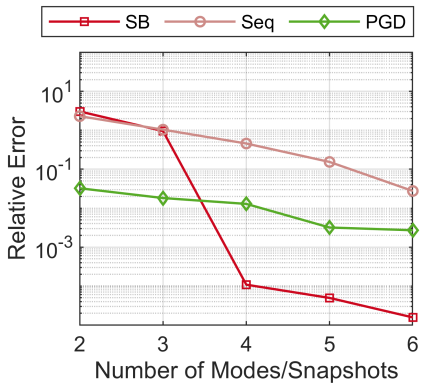

Fig. 12: Error of the MOR techniques for $\sigma = 40\,\mathrm{MS/m}$.

firstly, the PGD produces accurate results with less modes than the sequential POD, secondly, the overall accuracy of the POD is linearly improving, while the PGD does not converge as smoothly as the POD methods. The POD, regardless of the snapshot method, soughts most relevant information of the solution space into the projection and thus is able to converge to the reference after enough modes are enriched. Due to the fact that the PGD does not use reference solution its convergence might be worse than the POD's, because the basis of the PGD does not have to be orthogonal. However, the PGD has its advantages in terms of computational effort shown in Table I. It only has to solve NoM·maxNL equation systems in the offline stage and consequently NoT·NoM multiplications in the online stage. For even bigger reduction the decomposition can be improved leading to a better accuracy with less modes as well as a better nonlinear convergence in the enrichment process by orthogonalization of the basis [10]. The POD nonetheless has less operations in the offline stage for sequential snapshot method and more operations in the online stage, because the reference load vector has to be built and four projection operations are necessary. The first three projections are associated with (10) and the last is necessary to reproject the reduced solution into the reference system.Furthermore, the PGD is able to cope with the 'curse of dimensionality' by adding the material parameter of the conductivity to the decomposition [13] [14].

V. Conclusion

In this work two MOR techniques have been utilized in context of an eddy current problem. By applying the POD and the PGD on the $\mathbf{T}-\mathbf{\Omega}$ formulation an accurate reduced system could be achieved. The solutions for the eddy current losses, as well as the distribution of the field quantities are equivalent to the reference solution. Further a direct comparison between both methods has been conducted. The influence of the choosen snapshot as well as the influence of the conductivity on the convergence process has been shown in detail, leading to the conclusion that both methods are well suited in this context.

References

[1] T. Henneron, S. Clénet, "Model order reduction of quasi-static problems based on POD and PGD approaches," in Eur. Phys. J. Appl. Phys., vol. 64, Nov. 2013.

[2] T. Henneron, H. Mac and S. Clénet, "Error estimation of a proper orthogonal decomposition reduced model of a permanent magnet synchronous machine," in IET Science, Measurement & Technology, vol. 9, no. 2, pp. 172-177, Mar. 2015.

[3] Z. Qin, H. Talleb, Z. Ren, "A Proper Generalized Decomposition-Based Solver for Nonlinear Magnetothermal Problems,"in IEEE Trans. Magn., vol. 52, pp. 1-9, Feb. 2016.

[4] A. Nouy, "A priori model reduction through Proper Generalized Decomposition for solving time-dependent partial differential equations," Computer Methods in Applied Mechanics and Engineering, vol. 199, no. 23, pp. 1603-1626, 2010.

[5] S. Boehmer, E. Lange, and K. Hameyer, "Non-Conforming Sliding Interfaces for Relative Motion in 3D Finite Element Analysis of Electrical Machines by Magnetic Scalar Potential Formulation Without Cuts," *IEEE Transactions on Magnetics*, vol. 49, no. 5, pp. 1833-1836, May 2013.

[6] J. B. Manges, Z. J. Cendes, "A Generalized Tree-Cotree Gauge for Magnetic Field Computation," in IEEE Trans. Magn., vol. 31, no. 3, May 1995.

[7] L. Montier, A. Pierquin, T. Henneron, S. Clénet, "Structure Preserving Model Reduction of Low-Frequency Electromagnetic Problem Based on POD and DEIM," in IEEE Trans. Magn., vol. 53, no. 6, pp. 1-4, June 2017.

[8] T. Henneron and S. Clénet, "Model-Order Reduction of Non-Linear Magnetostatic Problems Based on POD and DEI Methods," in IEEE Transactions on Magnetics, vol.50, no. 2, pp. 33-36, Feb. 2014.

[9] V. Mukherjee, M. F. Far, F. Martin and A. Belahcen, "Constrained Algorithm for the Selection of Uneven Snapshots in Model Order Reduction of a Bearingless Motor," in IEEE Trans. Magn., vol. 53, no. 6, pp. 1-4, June 2017.

[10] T. Henneron, S. Clénet, "Application of the PGD and DEIM to Solve a 3-D Non-Linear Magnetostatic Problem Coupled With the Circuit Equations," in IEEE Trans. Magn., vol. 52, no. 3, pp. 1-4, March 2016.

[11] Z. Qin, H. Talleb, S. Yan, X. Xu, Z. Ren, "Application of PGD on Parametric Modeling of a Piezoelectric Energy Harvester," in IEEE Trans. Magn., vol.52, pp. 1-11, Nov. 2016.

[12] M. Farzamfar, P. Rasilo, F. Martin, A. Belahcen, "Proper orthogonal decomposition for order reduction of permanent magnet machine model," in 2015 18th International Conference on Electrical Machines and Systems (ICEMS), pp. 1945-1949, 2015.

[13] F. Chinesta, R. Keunings, A. Leygue, "The Proper Generalized Decomposition for Advanced Numerical Simulations," Springer International Publishing, 2014.

[14] A. Krimm, T. Casper, S. Schöps, H. De Gersem, L. Chamoin, "Proper Generalized Decomposition of Parameterized Electrothermal Problems Discretized by the Finite Integration Technique," in IEEE Trans. Magn., vol. 55, no. 6, 2019.